Evaporation of Ethanol/Water Droplets: Examining the Temporal Evolution of Droplet Size, Composition and Temperature

Rebecca J. Hopkins and Jonathan P. Reid*

School of Chemistry, University of Bristol, Cantock's Close, Bristol BS8 1TS, U.K.

Received: April 1, 2005; In Final Form: July 13, 2005

The evolving size, composition, and temperature of evaporating ethanol/water aerosol droplets 25−57 μm in radius are probed by cavity enhanced Raman scattering (CERS) and laser induced fluorescence. This represents the first study in which the evolving composition of volatile droplets has been probed with spatial selectivity on the millisecond time scale, providing a new strategy for exploring mass and heat transfer in aerosols. The Raman scattering intensity is shown to depend exponentially on species concentration due to the stimulated nature of the CERS technique, providing a sensitive measure of the concentration of the volatile ethanol component. The accuracy with which we can determine droplet size, composition, and temperature is discussed. We demonstrate that the CERS measurements of evolving size and composition of droplets falling in a train can be used to characterize, and thus avoid, droplet coagulation. By varying the surrounding gas pressure (7−77 kPa), we investigate the dependence of the rate of evaporation on the rate of gas diffusion, and behavior consistent with gas diffusion-limited evaporation is observed. We suggest that such measurements can allow the determination of the vapor pressures of components within the droplet and can allow the determination of activity coefficients of volatile species.

1. Introduction

A quantitative description of mass and heat transfer in aerosols is of importance in scientific disciplines as diverse as combustion science, and atmospheric chemistry and physics. Techniques for probing the evolution of aerosol particle size, temperature, and composition are essential to fully characterize the mechanisms of mass and heat transfer.[1] In addition, if the spatial inhomogeneities in composition and temperature that arise in a single particle during evaporation or growth can be explored, a rigorous assessment of current mass and heat transfer theories can be undertaken.

A wide range of experimental and theoretical studies has been undertaken to investigate mass transfer in aerosols, the majority of which investigate the evolution of an ensemble of particles.[2−4] Focusing more particularly on studies in which measurements are made on a single aerosol droplet rather than an ensemble, the evaporation of single-component and binary droplets have been examined by probing the evolving droplet size using elastic light scattering and fluorescence methods. Devarakonda et al. used elastic light scattering and Mie theory to examine the changing droplet size occurring as a result of evaporation for binary droplets composed of ethanol and methanol.[5] By probing a droplet train at various evaporation times, they were successful in extracting thermodynamic parameters such as vapor pressure and activity coefficients for alcohol droplets initially ∼11 μm in radius. Several groups have studied the evaporation of lower volatility droplets by monitoring the evolving size of a single droplet trapped in an electrodynamic balance using elastic light scattering. Davis et al. have studied the evaporation of several multicomponent systems including droplets composed of 1-bromotetradecane and 1-iodododecane, 1-octadecene and 1-bromohexadecane, and dibutyl phthalate and dioctyl phthalate.[6,7] Experiments have been typically performed on droplets 1−20 μm in radius. The influence of organic components on the evaporation of water droplets has received some limited attention.[8] Electrodynamic levitation and Raman spectroscopy have also been used to investigate the deliquescence and efflorescence of inorganic/aqueous aerosol particles.[9−11] In a recent study, Raman spectroscopy was used in addition to elastic light scattering to probe the deliquescence/efflorescence of single levitated $H_2SO_4/NH_3/H_2O$.[12] Raman spectroscopy has mostly failed to provide a quantitative measure of droplet composition, and in only a few examples have compositional measurements been possible.[13,14] Thus, the evolving droplet composition during mass transfer has proved challenging to monitor.

Fluorescence spectroscopy has been used to probe the evolving size of evaporating droplets. The evaporation rate of pure ethanol droplets of radius ∼30 μm has been investigated by Chang et al.[15] by doping the droplets with a fluorescent dye (Coumarin 481). Fluorescence is enhanced at resonant wavelengths commensurate with whispering gallery modes (WGMs), also known as morphology dependent resonances, providing a structured fluorescence spectrum that corresponds to a unique fingerprint of droplet size. By monitoring the resonant wavelengths within the fluorescence spectrum at various times following droplet production, they monitored the evolving size of the evaporating droplet, allowing the evaporation rate to be accurately determined. Using a similar approach, Pastel et al. measured the evaporation rates of 1−2 μm droplets of ethylene glycol doped with Rhodamine 590.[16] The size change of single droplets, which were trapped in a 20 μm hollow fiber by two counter propagating laser beams, was monitored by comparing the change in wavelength of WGMs to values obtained using Mie theory.

In this publication, we demonstrate that cavity enhanced Raman scattering (CERS) and laser induced fluorescence can be used to probe the evaporation of binary ethanol/water

* Corresponding author. E-mail: j.p.reid@bristol.ac.uk.

10.1021/jp0516543 CCC: $30.25
Published on Web 08/13/2005

droplets, providing information on evolving droplet size, composition and temperature. CERS not only enables droplet size to be measured but also allows droplet composition to be quantified with high accuracy and with spatial selectivity.[17−19] We examine the evaporation of a train of droplets in the size range 25−57 μm into a dry nitrogen atmosphere over a pressure range of 7−77 kPa. Under these conditions, which can be classified as falling within the continuum regime, gas diffusion limits the evaporative flux from the droplet.[20] By monitoring the evaporation of droplets produced in a droplet train, we can explore the evaporation of such highly volatile droplets at a short time after production (0.2−10 ms).

A spherical droplet behaves as a low loss optical cavity at wavelengths commensurate with WGMs. Such resonant modes occur when an integer number of wavelengths (the mode number, n) form a standing wave around the circumference of a particle, thus providing a mechanism for optical feedback.[15,21−23] Nonlinear stimulated Raman scattering (SRS) occurs only at wavelengths commensurate with WGMs and the Raman band has a structured, rather than a continuous, band profile.[18,19] The wavelengths of the WGMs can be used to determine the droplet size by performing Mie scattering calculations, as described previously.[24] The CERS spectral bands occur at specific Raman shifts characteristic of the chemical constituents of the droplet, providing a signature of composition in addition to size. The exponential rise in the SRS signal from a specific component with an increase in concentration provides an accurate method for determining droplet composition.[26−28] In addition, the SRS signal arises from the outer rim of the droplet, propagating from the interface to a depth of $\sim R_p/m$ measured from the droplet center, where R_p is the droplet radius and m is the real part of the refractive index.[29,30] The maximum propagation depth of light circulating within the droplet is determined by the depth to which the light can travel while still undergoing total internal reflection on encountering the interface. Thus, for a 30 μm radius water droplet, the SRS signal originates from the outer 7.5 μm shell of the droplet. The nonlinearity and the spatial selectivity of the SRS signal make the technique ideally suited for investigating the compositional changes accompanying droplet evaporation or growth.

In section 2 we describe the experimental technique and discuss the errors associated with the measurements. A description of the quantities measured is presented in sections 3.1 and 3.2, with reference to the standard formalism for droplet evaporation within the continuum regime. In section 3.3, measurements of the evaporation rates of ethanol/water droplets are presented and discussed in section 3.4. The objective of this study is to provide a benchmark test of the experimental technique allowing further research into mass and heat transfer to be conducted.

2. Experimental Technique

We first describe the experimental method and technique before discussing the accuracy with which droplet size, temperature, and composition can be determined.

2.1. Description of the Technique. The CERS experimental technique for determining the composition of alcohol/water droplets has been introduced in a previous publication.[17] The modified experimental apparatus used in this study is illustrated in Figure 1. A vibrating orifice aerosol generator (VOAG),[30] located within a regulated aerosol chamber, is used to generate a collimated train of droplets with a Gaussian size distribution of breadth ±200 nm at the full width half-maximum.[24] The piezoelectric crystal of the VOAG is modulated with a square-wave voltage of 0−20 V provided by a SRS DS335 signal generator, which acts to drive the oscillation of the crystal. A HeNe laser, focused to a beam waist estimated to be ~20 μm, is employed to monitor the stability of the droplet train by observing the elastic scattering diffraction pattern. The HeNe laser also serves to define the optical collection axis perpendicular to the propagation axis of the probe laser beam. This enables droplets to be reproducibly positioned in the focal waist of the pulsed Nd:YAG laser and allows reproducible alignment of the Raman scattered light with respect to the spectrograph entrance slit.

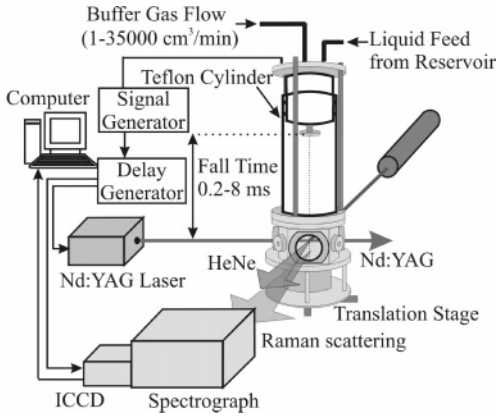

Figure 1. Experimental apparatus, illustrating that droplets can be reproducibly positioned in the focal waist of the pulsed Nd:YAG laser allowing reproducible alignment of the Raman scattered light with respect to the spectrograph entrance slit. The ICCD, laser pulse and droplet generation are synchronized.

A Continuum Surelite Nd:YAG laser operating at the tripled fundamental wavelength (355 nm) is focused to a beam waist comparable in size to the droplet being illuminated, ensuring that only a single droplet is illuminated. Laser pulse energies greater than 1 mJ lead to optical saturation effects and laser induced breakdown and these effects have been discussed in earlier publications.[26,31] Thus, pulse energies between 100 and 800 μJ are used in this work with the majority of measurements made with a pulse energy of 200 μJ. The laser delivers pulse energies of up to 100 mJ. This is first reduced to 1% by using the back reflection from an uncoated BK7 window to illuminate the droplet. Fine control in pulse energy can then be achieved by varying the time delay between the laser flashlamps and Q-switch. The aerosol chamber is mounted on a xy translation stage, allowing the droplet train to be translated in two independent horizontal directions with respect to the laser beam and collection axis. Thus, preferential edge illumination of the droplet is possible.[32]

The laser pulse, droplet generation, and gating of an intensified CCD (Princeton Instruments PI-MAX camera) are synchronized to allow the CERS signal from a single droplet to be collected. Single laser pulse, single droplet CERS spectra are collected with a 0.5 m focal length Acton SpectraPro 500i spectrograph equipped with a 2400 g mm^{-1} diffraction grating providing high-resolution wavelength dispersion (0.012 nm/CCD pixel). Spectra are collected over a wavelength range of 391−408 nm. This range encompasses both the CH and OH Raman signals from ethanol and water at wavelengths centered at 395.6 and 403.8 nm, respectively, corresponding to Raman shifts of 2900 and 3400 cm^{-1}, respectively. Composite CERS spectra for compositional analysis were generated by the addition of ~500 single droplet CERS spectra. Both single laser shot and composite CERS spectra are illustrated in Figure 2. This signal accumulation procedure leads to a signature of composition

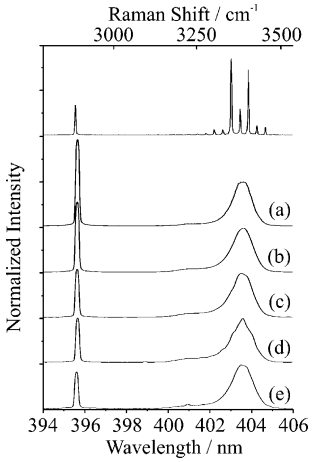

Figure 2. CERS composite spectra for 37.8 μm radius 18% v/v ethanol/water droplets at 0.2, 0.8, 1.3, 1.7 and 2.0 ms after generation ($a - e$, respectively), evaporating in a dry nitrogen atmosphere at 13.2 kPa. A CERS fingerprint from a single ethanol/water droplet is shown for comparison.

averaged over variations in droplet size and laser alignment. The resulting spectrum has a smooth CERS band contour: the extremely sensitive dependence of WGM wavelengths on droplet size leads to an average composite CERS band with no residual structure.

The time taken for the droplets to fall into the laser probe region, and thus their velocity, was characterized using an elastic light scattering method under the full range of conditions used in this study. The signal generator alternates between two frequencies, generating two droplet sizes. A HeNe laser interrogates the droplets at a known distance from the generation region. The elastically scattered light from the droplets is monitored using a photodiode, with the resultant signal recorded on a TDS 3034B Tektronix oscilloscope. The fall time is determined by the time delay between the change in droplet size at the generator and the detection of a change in elastic scattering intensity at the fall height, as illustrated in Figure 3a. The fall time is measured at varying distances from the droplet generator, with the gradient of a plot of fall distance against fall time yielding the droplet velocity as illustrated in Figure 3b. The velocity of droplets under the conditions used in this study was determined as 10 ± 1 m s^{-1}, and droplets were probed at fall times varying between 0.2 and 10 ms.

The aerosol chamber has been described in detail in an earlier publication.[33] The droplet evaporation time is varied by changing the distance between the droplet generation region and probe laser by translating the aerosol generator vertically. Utilizing the regulated aerosol chamber, we introduce the ethanol/water droplets into a dry nitrogen atmosphere at a pressure within the range 7−77 kPa. Nitrogen is passed through the chamber at a flow rate of 5000 cm^3 min^{-1}. Experiments were conducted to ensure that the flow rate of the gas phase had no impact on the evaporation of the droplet and to avoid the departed flux from previously sampled droplets influencing the evaporation of subsequent droplets. The integrated intensity ratio of the CH to OH band, providing a measure of droplet composition, was measured at nitrogen flow rates over the range 1000−5000 cm^3 min^{-1} at a fall time of 5 ms. This measurement was made at 13 and 73 kPa, and the results are presented in Figure 4. Invariance in the integrated intensity ratio of the CH to OH band with nitrogen flow rate is observed, suggesting the flow rate of the gas through the chamber has no impact on droplet evaporation.

2.2. Determination of Droplet Size, Composition, and Temperature. We have illustrated in a previous publication

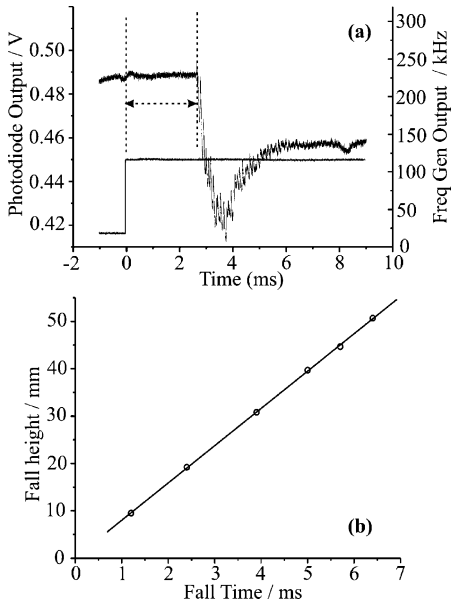

Figure 3. (a) An example of a droplet fall time measurement. The fall time is indicated by the arrow and is determined by the delay in the elastic light scattering intensity as measured by a photodiode from time zero. The step in frequency is shown at time zero with the modulation frequency displayed on the right axis. The elastic light scattering intensity is given by the left axis. (b) Variation in fall height with fall time allowing the determination of fall velocity.

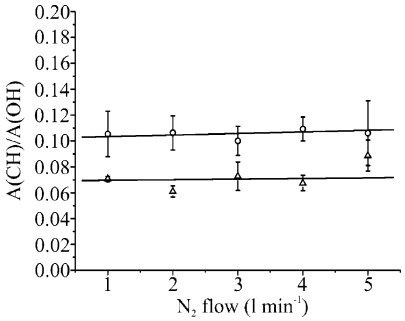

Figure 4. Invariance of area of the CH to OH CERS band with N_2 flow at two chamber pressures, 13 and 73 kPa (triangles and circles respectively). The lines represent the best linear fit to the data.

that CERS can be used to simultaneously determine the size and composition of ethanol/water droplets.[17] The accuracy by which we are able to determine particle size from a CERS spectral fingerprint from a single droplet has also been discussed in detail.[24] The compositional and temperature changes experienced by an evaporating droplet will clearly reduce the accuracy with which the droplet size can be determined by giving rise to an uncertainty in the refractive index of the droplet. The maximum change in ethanol concentration from evaporation in this work is ~1% v/v in the range 17−18% v/v. Taking the uncertainty in composition to be ±1% v/v, the uncertainty associated with the calculated droplet radius can be shown to increase from 2 nm for a 10 μm radius droplet to 6 nm for a 40 μm radius droplet, reflecting an uncertainty in the refractive index of 7.5×10^{-4}. Over the temperature range 273−303 K the refractive index of the ethanol/water mixture varies from 1.345 to 1.342.[34] Taking this range as a reflection of the uncertainty in droplet refractive index, the uncertainty associated with the calculated droplet radius increases from 10 nm for a 10 μm radius droplet to 100 nm for a 40 μm radius droplet. Thus, the uncertainties in refractive index arising from compositional and temperature changes in the droplet lead to errors that are similar to the estimated uncertainties that arise from

the spectral resolution and wavelength accuracy of the spectrograph/ICCD.[24] More importantly, all of these uncertainties are smaller than the breadth of the size distribution generated by the VOAG, which precludes an accurate measurement of size change due to evaporation. Thus, the errors in size determination arising from uncertainty in composition and temperature can be ignored. Sizes are quoted to an accuracy of 0.1 μm and an associated breadth in size distribution of $\pm$200 nm should be assumed.

The nonlinear character of SRS stipulates that the CERS signal is exponentially dependent on species concentration under optically unsaturated conditions.[25] Unsaturated conditions occur when the pump photons trapped within the aerosol droplet are not significantly depleted by the Raman scattering process and all experiments were performed under this regime. The exponential relationship between SRS signal amplitude and species concentration provides an extremely sensitive method for measuring droplet composition. A calibration curve is first formulated by using the OH peak intensity as an internal reference and by comparing the integrated intensity ratio of the CH to OH Raman bands with varying composition in measurements made at atmospheric pressure.[17] The CH (395−396 nm) and OH (400−405.5 nm) bands are integrated over their full spectral range to calculate the calibration ratio. There is no contribution to the SRS OH band from ethanol for droplets composed of ethanol/water, and this has been measured over a wide range of ethanol concentrations including pure ethanol. The sensitivity in measuring droplet composition for the two pump wavelengths of 532 and 355 nm has been explored in previous work and it was concluded that the pump wavelength of 355 nm offered the greatest sensitivity.[17] At this wavelength, the CH to OH intensity ratio increases by 2 orders of magnitude over the ethanol concentration range 16−18% v/v. This allows the composition to be determined with an estimated accuracy of $\pm$0.2% v/v.

An example of the accuracy with which composition can be determined is illustrated in Figure 2, which shows the evolution in the composite CERS spectrum with time for droplets of radius 37.8 μm evaporating in a dry N_2 atmosphere at 13.2 kPa. All spectra are normalized to the maximum intensity of the OH band. The intensity of the CH Raman stretching band decreases in magnitude relative to the OH band with increase in time, demonstrating that the more volatile alcohol evaporates more rapidly from the droplet than the less volatile water component. The equivalent change in alcohol concentration corresponds to a decrease from 17.9 $\pm$ 0.2% v/v to 17.1 $\pm$ 0.2% v/v over 2 ms.

The size independence of the integrated intensity ratio of the CH to OH Raman bands has been investigated over the size range 20−35 μm at a pump wavelength of 532 nm.[17] The current study has examined the effect of a broader droplet size range on the integrated intensity ratio of the CH to OH bands using a pump wavelength of 355 nm. These results are presented in Figure 5 as calibration curves. Complications introduced by evaporative losses were avoided by measuring the calibration plots at atmospheric pressure and a short exposure time of 0.2 ms. To maintain approximately the ratio between laser beam waist and droplet radius, the focal length of the lens used was varied from 10 cm for the 20 and 35 μm radius droplets to 50 cm for the >50 μm radius droplets.

There is no systematic variation in the integrated intensity ratio for droplets of radius 20 and 35 μm. A linear fit through the data for both of these droplet radii is presented in Figure 5, coupled with maximum and minimum linear fits as determined from the intercept error. An estimated accuracy in composition determination of $\pm$0.2% v/v can be determined from the maximum and minimum linear fits for these droplet sizes. The calibration plot for droplets of 50 μm radius is treated separately. It is clear that there is a change in integrated intensity ratio for droplets in this larger size regime as a consequence of a reduced intensity illuminating the droplet resulting from the use of a longer focal length lens and a larger focal waist. In the evaporation measurements that follow, this calibration curve was used for measurements of the evaporation of >50 μm radius droplets. All other measurements for other droplet sizes were performed with the shorter focal length lens and the former calibration curve was used.

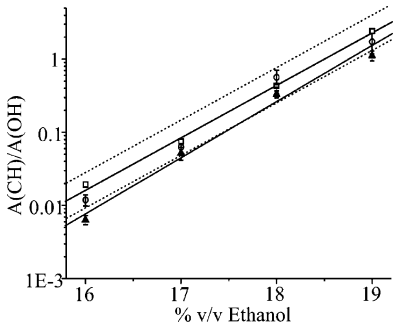

Figure 5. Calibration curves for the variation in the ethanol CERS signal with composition for three droplet radii, 20, 35 and 50 μm (circles, squares and triangles respectively). The upper solid line is a linear fit through the data for both the 20 and 35 μm radius droplets and the dashed lines are the maximum and minimum linear fits as determined from the intercept error. The lower solid line is a linear fit through the 50 μm radius droplet data.

Droplet temperature is characterized by laser induced fluorescence.[35] Multicomponent ethanol/water droplets are doped with Rhodamine B at a concentration of 1×10^{-6} M, which exhibits a temperature dependent fluorescence spectrum. Droplet fluorescence spectra were collected using the 300 g mm^{-1} diffraction grating over the wavelength range 520−680 nm. Conformity of fluorescence band shape recorded from the droplet and bulk phases is essential and has been thoroughly investigated. By comparison with a bulk-phase calibration, the fluorescence spectrum from the evaporating droplets can be used to determine droplet temperature with an associated error estimated to be better than $\pm$1 K. On the time scale of the measurements presented here ($\sim$10 ms), the Rhodamine B can be assumed to be homogeneously mixed through the entire droplet volume. Although for the fluorescence and Raman spectroscopy measurements the laser might be expected to perturb the droplet temperature, this does not appear to occur on the time scale of the measurement with the droplet temperature recorded from the Rhodamine B fluorescence equivalent to the ambient temperature within $\pm$1 K. The fluorescence technique for measuring the droplet temperature will be discussed in more detail in a separate publication.

3. Results and Discussion

The evaporation of a multicomponent droplet is a complex process to study. Davis and co-workers have outlined the phenomena that must be accounted for.[7] An understanding of the diffusional transport of molecules within the droplet and in the surrounding gas phase is crucial. The rapid evaporation of highly volatile components can lead to nonisothermal behavior, with the surface undergoing a more rapid fall in temperature than the interior as the droplet undergoes evaporative cooling.[36] A steep temperature gradient is established near the interface

and the surface temperature falls until the rate of heat transfer between the particle and surrounding gas phase balances.[37] Until this steady state is achieved, unsteady evaporation kinetics are followed, with the evolution in droplet size, composition and temperature with time leading to a temporal variation in the evaporation rate. In addition, Stefan (or convective) flow must be considered under such conditions. Most evaporation studies using droplet trains have considered that quasi-steady-state evaporation can be assumed.[38] However, in recent measurements made within 1 ms of droplet generation, Devarakonda and Ray have more accurately considered the evaporation of droplets produced by a VOAG to be unsteady and have included a correction term, η, for the interparticle interactions that occur between adjacent particles within the train.[37] We adopt their approach in this work.

3.1. Evaporation in the Continuum Regime. In the evaporation measurements performed in this study, the mean free path of molecules in the surrounding gas phase, λ, is considerably shorter than the radius of the droplet, R_p. This is characterized by the Knudsen number, *Kn*.[36]

$$Kn = \frac{\lambda}{R_p} \tag{1}$$

The Knudsen number, as calculated from the range of pressures (9−73 kPa) and droplet sizes (26−57 μm) used in this work, has a value between 4×10^{-2} and 2×10^{-3}. Thus, even at the lowest pressure of 9 kPa and the smallest droplet radius of 26 μm, $Kn \ll 1$ and the evaporation is limited by gas diffusion.[36]

The instantaneous flux (moles time^{-1}) of species *i* away from a droplet can be determined from considering the interfacial mass balance:[6]

$$\frac{dn_i}{dt} = -2\pi R_p \eta Sh D_{g,i}\left[\frac{\gamma_i x_i p_i(T_s)}{RT_s} - \frac{p_{i,\infty}}{RT_\infty}\right] \tag{2}$$

where $D_{g,i}$ is the diffusion coefficient of the vapor of species *i* in the surrounding bath gas, *Sh* is the Sherwood number, which accounts for the correction in mass transfer that must be included when considering a falling droplet instead of one that is stationary, and η is the correction for interparticle interactions. The activity coefficient of species *i* is denoted by γ_i, the mole fraction by x_i, and the vapor pressure of the component *i* at the surface of the droplet with a surface temperature of T_s by $p_i(T_s)$. The partial pressure of component *i* in the gas phase at an infinite distance from the droplet is denoted by p_∞, and the temperature of the gas phase by T_∞. Thus, the flux of ethanol from the droplet into dry nitrogen ($p_{i,\infty} = 0$) can be written as

$$\frac{dn_{EtOH}}{dt} = -2\pi R_p \eta Sh D_{g,EtOH} \frac{\gamma_{EtOH} x_{EtOH} p_{EtOH}(T_s)}{RT_s} \tag{3}$$

with a similar expression for the flux of water from the droplet. The variation in the diffusion coefficient of ethanol with nitrogen pressure, p_{N_2} (in kPa), can be calculated from the diffusion constant of ethanol in dry nitrogen, D_{EtOH,N_2}, of 1.04×10^{-3} kPa m^2 s^{-1}.[39]

$$D_{g,EtOH} = \frac{D_{EtOH,N_2}}{p_{N_2}} \tag{4}$$

In the measurements presented here, the change in droplet radius is ≪1% of the initial droplet radius and we can therefore determine the time dependence of the number of moles of ethanol remaining in the droplet from eq 3 simplified to the following form,

$$n_{EtOH} = n^0_{EtOH} - \frac{2\pi R_p \eta Sh D_{g,EtOH}}{R}\int_0^t \frac{\gamma_{EtOH} x_{EtOH} p_{EtOH}(T_s)}{T_s}\,dt \tag{5}$$

where the superscript zero denotes the starting value of the number of moles of ethanol in the droplet. Under unsteady conditions, the activity coefficient, mole fraction of ethanol, vapor pressure of ethanol and surface temperature are dependent on time. We now move on to discuss the temporal measurements of the droplet composition, size, and temperature that have been performed, which can yield important insights into the key processes occurring under unsteady conditions. By varying the surrounding nitrogen pressure, we are also able to demonstrate that the evaporation is occurring within the continuum regime and are able to estimate the vapor pressure of ethanol in the droplet.

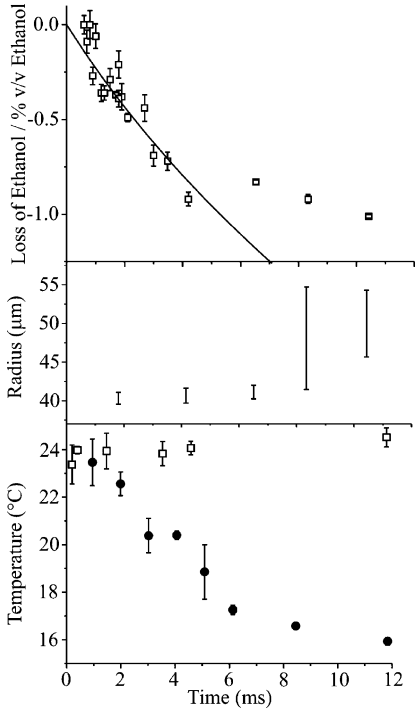

Figure 6. Depletion of ethanol concentration with time and the corresponding change in the droplet size distribution. A calculation based on the quasi-steady treatment of ref 38 is shown by the solid line. Coagulation of droplets in the droplet train at times later than 6 ms is evident. Droplet temperature is measured at two pressures. Droplets were 40.2 μm in radius, evaporating into an atmosphere of dry nitrogen at 77 and 7 kPa (squares and circles respectively).

3.2. Characterization of Droplet Coagulation in the Aerosol Train. The magnitude of deceleration experienced by falling droplets depends on both droplet size and velocity.[37] This deceleration effect has implications for performing time dependent evaporation studies with a droplet train apparatus. Droplets 40.2 μm in radius, with a fall velocity of ∼10 ± 1 m s^{-1} and an initial separation estimated to be $\sim 6 \times 10^{-5}$ m, were introduced into a dry nitrogen atmosphere at 77 kPa. The time dependence in the ethanol concentration was measured under these conditions over a ∼10 ms period, showing a reduction in ethanol fraction from 18.6% v/v to 17.6% v/v; this is illustrated in Figure 6. After this time, there is a change in the temporal behavior of the integrated CERS intensity ratio, and it becomes approximately invariant within the associated error.

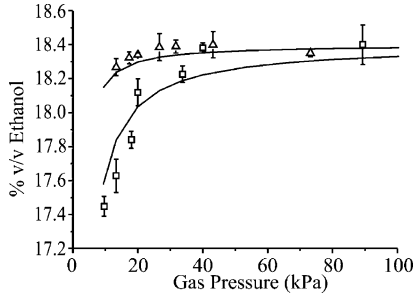

Figure 7. Variation in ethanol concentration with nitrogen gas pressure probed at 0.2 ms for droplets of radius 29 and 57 μm (squares and triangles, respectively). Calculations based on the quasi-steady treatment of ref 38 are shown by the solid line.

A droplet size distribution was determined at each fall time from the individual CERS fingerprints of which the composite spectra are composed and is also shown in Figure 6. The increase in the average size in the distribution after 6 ms can be attributed to the disparity in deceleration of different droplets, leading to the eventual coagulation of two sequential droplets in the train. The droplet radius increases from a mean value of $\sim 40 \pm 1$ to $\sim 50 \pm 4$ μm, and a simple calculation of the volume of each droplet reveals that this is the result on average of two droplets coagulating. The change in the evaporation rate apparent in Figure 6 following coagulation is a consequence of the change in surface area-to-volume ratio for the droplets prior to and after coagulation.

In addition to measuring both the changing size and composition of droplets in the aerosol train at various fall times, the evolution in droplet temperature during the unsteady evaporation has also been determined by laser induced fluorescence. Droplets were probed under the same experimental conditions used for the size and composition measurements with a dry nitrogen pressure of 77 kPa, and also at a reduced pressure of 7 kPa. These results are presented in Figure 6. A decrease in droplet temperature of 7.5 ± 1 °C is measured at 7 kPa, whereas at the higher pressure used for the size and composition measurements, invariance in droplet temperature is observed. The evaporative flux is greater at lower pressures, resulting in a higher degree of evaporative cooling. The invariance in temperature occurring at the higher pressure indicates that although the droplet is evaporating, as seen from the change in composition, the evaporation rate is not sufficient to lead to significant evaporative cooling. It should be noted that the temperature measurements provide an average droplet temperature and are not particularly sensitive to the depression in surface temperature that occurs.

3.3. Gas-Diffusion-Limited Evaporation. To assess the potential of using the CERS technique to quantitatively probe evaporation dynamics, we have investigated the dependence of the droplet composition on the pressure of dry nitrogen surrounding the droplets. Measurements have been made for droplets of a range of sizes (26 to 57 μm radius) and initially containing 18.4% v/v ethanol at a time of 0.2 ms following generation. The concentration of ethanol remaining in the droplet after this time provides a measure of the relative fluxes of ethanol and water away from the droplet.

The dependence of the final ethanol concentration on gas pressure is illustrated in Figure 7 for two droplet sizes. Ethanol and water evaporate from the droplet at different rates; ethanol has a higher vapor pressure than water and evaporates from the droplet at a greater rate. It is evident that reducing the pressure of dry nitrogen surrounding the droplet increases the gas diffusion rate, thus increasing the evaporative flux of ethanol and water from the droplet.

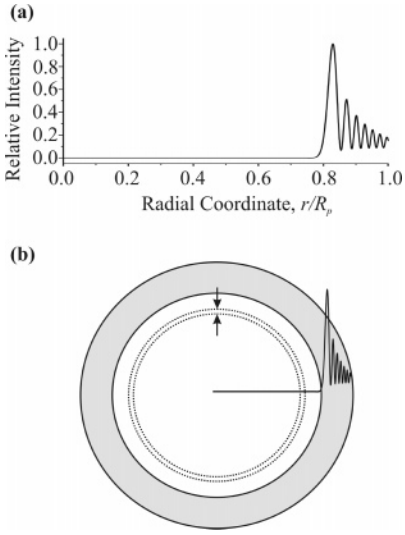

Figure 8. (a) Calculated radial dependence, r, of the internal field intensity for a WGM of mode order l=7, illustrating that the light intensity is concentrated at distances greater than $r > 0.75R_p$ (or R_p/m) from the droplet center.[26] (b) Schematic showing the CERS signal volume (shaded gray) as a fraction of the total volume and the distance over which a ethanol molecule can diffuse (between the two concentric dashed circles) during the time scale of the measurement (0.2 ms).

The decrease in ethanol concentration, $\Delta\%V_{EtOH}$, can be determined from the initial concentration and the ethanol remaining in the droplet after 0.2 ms. Thus, we must relate eq 5 to the $\Delta\%V_{EtOH}$. This is considered in the Appendix and eq 5 can be written in the form

$$\Delta\%V_{EtOH} = -100\,\frac{V_{mEtOH}}{V_{total}}\,\frac{2\pi R_p \eta Sh D_{g,EtOH}}{R}\int_0^t \frac{\gamma_{EtOH} x_{EtOH} p_{EtOH}(T_s)}{T_s}\,dt \quad (6)$$

where V_{total} is the total volume of the droplet. This can be written as

$$\Delta\%V_{EtOH} = -100\,\frac{3V_{mEtOH}\eta Sh D_{g,EtOH}}{2R_p{}^2 R}\int_0^t \frac{\gamma_{EtOH} x_{EtOH} p_{EtOH}(T_s)}{T_s}\,dt \quad (7)$$

It should be noted that no change in droplet radius over the experimental conditions used was measured. The aerosol generation produces a droplet size distribution of $\pm$200 nm, so any change in droplet radius occurring due to evaporation is $<$200 nm. Over the droplet radius range examined in this experiment, the change in volume due to a decrease in droplet radius of 200 nm equates to volume changes of 1.66×10^{-15} m^3 from an initial volume of 7.36×10^{-14} m^3 for a 27 μm radius droplet, and 8×10^{-15} m^3 from 7.8×10^{-13} m^3 for a 57 μm radius droplet. As this volume change is small ($<$3%), it is assumed that the partial molar volumes of ethanol and water and the total droplet volume are the same at the start and finish compositions, i.e., $V_{mEtOH} \sim V^{\circ}_{mEtOH}$ and also $V_{total} \sim V^{\circ}_{total}$.

It is necessary to consider the depth probed from the droplet interface by the CERS measurements. As an example, an internal field calculation has been performed for an $l = 7$ resonance expected to be typical of those contributing to the CERS signal for the droplet sizes investigated here.[26,40] This is illustrated in Figure 8a. This shows that the signal volume is located in the

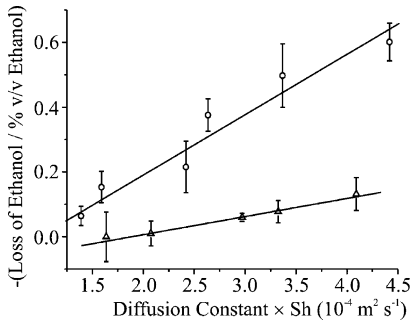

Figure 9. Correlation between the magnitude of the change in ethanol concentration of the droplet at 0.2 ms and the (gas diffusion constant × Sherwood number) for droplets of radius 29 and 57 μm (circles and triangles, respectively).

outer shell of the droplet, penetrating to a depth of R_p/m, or 0.75 R_p. Thus, the signal volume represents a fraction of the total droplet volume, W(Signal), given by

$$W(\text{Signal}) = \frac{R_p^3 - (R_p/m)^3}{R_p^3} \sim 0.58 \quad (8)$$

On the time scale of the measurements (0.2 ms) the diffusion distance of an ethanol molecule in the bulk of the droplet is calculated to be 0.6 μm from the liquid-phase diffusion coefficient of ethanol (1.43×10^{-5} cm^2 s^{-1}).[39] This is considerably less than the R_p/m distance, as is illustrated in Figure 8b and indicates that the change in composition in this outer shell does not reflect accurately the total droplet compositional change. To account for this, all subsequent compositions $\%V_{EtOH}$ are weighted by the signal and core volume fractions, W(Signal) and W(Core), according to the equation

$$\%V_{EtOH}(\text{Weighted}) = W(\text{Signal})\%V_{EtOH}(\text{Signal}) + W(\text{Core})\%V_{EtOH}(\text{Core})$$
$$= 0.58\%V_{EtOH}(\text{Signal}) + 0.42\%V_{EtOH}(\text{Core}) \quad (9)$$

where $\%V_{EtOH}$(Weighted) is the volume weighted composition, $\%V_{EtOH}$(Signal) is the measured composition and $\%V_{EtOH}$(Core) is the core composition, which is equal to the initial composition of the droplet.

Although a full time dependence of the evaporation with varying pressure and droplet size would allow a complete evaluation of the integral in eq 7, in this work we make the assumption that the change in surface temperature, and thus the change in vapor pressure, is negligible. Future work will address this more thoroughly to account for the unsteady evaporation rate, but such an approximation is reasonable over the 0.2 ms time frame used here. Within this approximation, eq 7 can be written as

$$\Delta\%V_{EtOH} = \left\{-100\frac{3V_{mEtOH}\Delta t}{2RT_s}\gamma_{EtOH}x_{EtOH}p_{EtOH}(T_s)\right\}\frac{\eta}{R_p^2}D_{g,EtOH}Sh \quad (10)$$

Thus, for a particular droplet size, the depletion of $\Delta\%V_{EtOH}$ should show a linear dependence with $Sh\ D_{g,EtOH}$ at a fixed droplet exposure time. This is observed in our experimental results, as illustrated in Figure 9. The change in ethanol concentration with varying diffusion constant is measured for five droplet radii ranging from 26 to 57 μm. The Sherwood number can be estimated from the Reynolds number, Re, and Schmidt numbers, Sc, as shown below:[5]

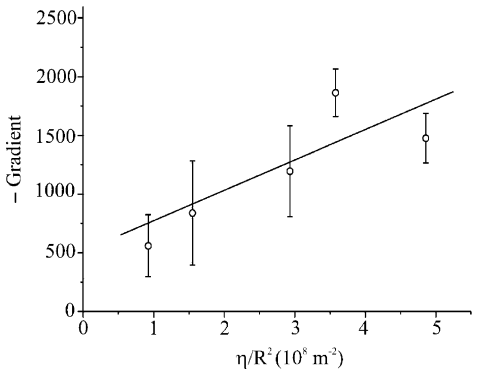

Figure 10. Variation in the gradient of plot in Figure 8 with η/(droplet radius)^2, allowing the vapor pressure at the surface of the droplet to be determined. (Note: The gradient has a negative value).

$$Sh = 2 + 0.6\sqrt{Re}\sqrt[3]{Sc} \quad (11)$$

The Reynolds and Schmidt numbers are defined as follows:

$$Re = \frac{v_t 2R_p}{\nu_{air}} \quad (12)$$

$$Sc = \frac{\nu_{air}}{D_g} \quad (13)$$

where v_t and ν_{air} are the terminal velocity of the droplet and the kinematic viscosity of air, respectively. Thus Sh is dependent on both the droplet diameter and $D_{g,EtOH}$ and is therefore factored into every measurement of $\Delta\%V_{EtOH}$.

From eq 10, the gradient of the dependence of ethanol depletion on $D_{g,EtOH}$ Sh should show a linear dependence on η/R_p^2, i.e.

$$\frac{d(\Delta\%V_{EtOH})}{d(ShD_{g,EtOH})} = -100\frac{3V_{mEtOH}\Delta t}{2RT_s}\gamma_{EtOH}x_{EtOH}p_{EtOH}(T_s)\frac{\eta}{R_p^2} \quad (14)$$

This is illustrated in Figure 10 which shows the variation in the gradient, taking the rate of ethanol evaporation with change in diffusion coefficient for five droplet diameters. η is the interaction parameter and accounts for the interparticle interactions occurring between evaporating droplets.[37] Devarakonda and Ray determined an empirical relationship for the dependence of η on the dimensionless spacing between droplets (i.e., l/R_p),[5]

$$\eta = -0.0078 + (0.07874(l/R_p)) \quad (15)$$

where l is the distance between droplet centers. l is calculated using $l = v/f$, where v is the droplet velocity and f modulation frequency of the piezoelectric crystal of the VOAG. To maintain the interaction parameter at a constant value in this work, l/R_p was kept at a constant value in all of the measurements presented here and is calculated to be 3.8 ± 0.5.

3.4. Assessment of the Experimental Technique. To assess the value of the experimental technique, it is possible to estimate the vapor pressure of the droplet from the gradient of the variation shown in Figure 10, i.e.

$$\text{Gradient} = \left\{-100\frac{3V_{mEtOH}\Delta t}{2RT_s}\gamma_{EtOH}x_{EtOH}p_{EtOH}(T_s)\right\} \quad (16)$$

It should be stressed that this provides a very approximate estimation of the vapor pressure subject to considerable approximation. From these results, we calculate $\gamma_{EtOH}x_{EtOH}p_{EtOH}(T_s)$ at the droplets surface to be 3.5 ± 1 kPa. Ethanol−water exhibits a large positive deviation from Raoult's law.[41] The vapor pressure of ethanol in a binary mixture of ethanol−water with a concentration of 18.4% v/v can be estimated to be 1.85 kPa from measurements made at 25 °C,[42] a factor of ∼2 lower that the value estimated in this work, yet higher than the value estimated from Raoult's law of 1.2 kPa. Clearly, the vapor pressure estimated from these data is an overestimate by a factor of ∼2 and it is necessary to consider the errors associated with such a measurement.

We first consider an additional error in the determination of the droplet composition that has not already been discussed. The time-evolution of the OH band shape shows a broadening on the low wavelength, low Raman shift edge over the time scale of the measurements shown in Figure 2, with the shoulder below 402.3 nm contributing only 5% to the full OH band integral at 0.2 ms and 7% at 2 ms. For the compositional measurements presented here, even with the maximum broadening evident at the longest evaporation times, the change in the integral of the OH band intensity leads only to a contribution to the error in $\%V_{EtOH}$ of ±0.1%. Thus, at the early times at which the vapor pressure is determined here, the broadening of the OH band does not have any effect on the compositional determination. The band broadening reflects a depression in the near surface temperature during the course of the evaporation and will be used in future work to determine the near-surface temperature. The line shape, frequency, and position of the spontaneous OH band has been shown to be sensitive to the local hydrogen-bonding environment, and hence, the OH band shape is sensitive to temperature.[43−45] By scaling spontaneous Raman bands to fit the SRS bands, it should be possible to determine the near surface temperature. Such a scaling procedure has already been demonstrated to work for ion doped droplets, confirming that the hydrogen bonding environment probed in droplets by SRS is consistent with that observed in the bulk phase.[27]

Perhaps the largest uncertainties arise from the corrections that have been made for the CERS signal volume and the interaction parameter for the droplet train. Although we believe we have made a justifiable estimate of the CERS signal volume, the CERS signal arises from the double resonance excitation of stimulated Raman scattering and is dependent on the overlap of the input and output resonant mode volumes.[40] This has a tendency to narrow the radial extent of the signal volume and the signal may arise from a region closer to the surface than is predicted by the R_p/m ratio. In addition, the interaction parameter is dependent on the interparticle separation in the droplet train. We have used an empirical estimate of the interaction parameter,[37] but an underestimate of the interaction parameter would lead to an overestimate of the vapor pressure by a directly proportional amount. Thus, it is unlikely that an overestimate of the vapor pressure by a factor of 2 could be accounted for by an error in the estimate of this parameter, although the interaction of droplets in the droplet train is almost certain to have an impact on the vapor pressure determination. This will be investigated further in subsequent work

It is also important to comment on the failings of the steady-state treatment adopted here. As the droplet evaporates, a substantial cooling of the droplet interface is to be expected. This will lower the vapor pressure of the ethanol and water components below that quoted above. In addition, the surface composition is likely to be lower than that measured due to the disparity in the diffusion distance on the time scale of the measurement and the signal depth. Applying a similar analysis to that discussed above that led to eq 8, the surface composition can be estimated to be ∼11% v/v for the smallest droplets evaporating at the lowest pressure. Both the temperature depression and the surface composition would act to increase the discrepancy between the literature vapor pressures and that measured, with the largest error arising in the measurements made at the lowest pressures for the smallest droplets. However, systematic errors in the signal volume and the interaction parameter are most likely to counter this, with the signal volume likely to be an overestimate and the interaction parameter likely to be underestimated.

With the complexity of the surface cooling and concentration effects, and uncertainty in the signal volume and the interaction parameter, a more quantitative estimate of the uncertainties associated with each of these is not tractable here and a detailed analysis using existing treatments for the evaporation of multicomponent droplets is essential.[1,38] A first step has been made in this direction by performing calculations based on the quasi-steady treatment of ref 38. The calculated results are compared to the experimental measurements in Figures 6 and 7 using a single scaling parameter to account for the fact that CERS probes only a fraction of the total droplet volume. Agreement is good for both the pressure and time dependent measurements and a similar level of agreement is observed for all of the data presented in this publication. A more complete discussion of this will be presented in a subsequent publication.

4. Concluding Remarks

We have discussed a novel experimental strategy for probing the evaporation dynamics of multicomponent ethanol/water droplets and we have demonstrated that it is possible to measure the evolving composition, size, and temperature of ethanol/water droplets by CERS and LIF. This complements the technique developed in earlier work by Vehring et al. that probed the evolving bulk composition of aqueous droplets by linear Raman spectroscopy.[13] In this work, the application of stimulated Raman scattering provides a sensitive approach for probing the evolving near-surface composition. This study has proven to be a benchmark of our experimental technique. Although quantitative agreement between the measured and literature vapor pressures is only within a factor of 2, further studies will seek to investigate the origin of this difference.

The composition range that can be accessed by CERS is rather limited in this publication due to the exponential relationship between species concentration and CERS signal. However, we can tune the composition range to which we are sensitive by varying the pump laser wavelength. In addition, recent work conducted in our laboratory has demonstrated that compositions from 10 to 90% v/v alcohol can be accessed using a broadband dye pump laser. As described earlier, we are also currently developing CERS to measure the surface temperature of the droplet, which can then be compared to the average droplet temperature as determined by the LIF technique. Knowledge of the surface and average droplet temperature under various experimental conditions will provide important information on temperature gradients within the droplet allowing a fuller appreciation of unsteady evaporation. The techniques outlined in this publication will also be applied to optically trapped aerosol droplets,[46] which will enable the problems associated with interdroplet coupling to be removed.

Acknowledgment. We acknowledge the financial support provided by the NERC within the Core Measurements for Atmospheric Science program. Also Dr. Robert Sayer for assisting with preliminary measurements, Dr. Chris Howle for his help at the conclusion of this work and Mr. Tony Rothin for design and fabrication of the aerosol generator and flow chamber.

Appendix

The $\Delta\%V_{EtOH}$ in a droplet composed of both ethanol and water can be defined:

$$\Delta\%V_{EtOH} = \%V_{EtOH} - \%V^0_{EtOH} \quad \text{(A1)}$$

where $\%V_{EtOH}$ is the % v/v ethanol remaining in the droplet at time t, and $\%\ V^0_{EtOH}$ is the % v/v ethanol initially. The percentage volume of ethanol present in the droplet is defined as

$$\%V_{EtOH} = \frac{V_{m,EtOH}n_{EtOH}}{(V_{mH_2O}n_{H_2O}) + (V_{m,EtOH}n_{EtOH})}100 \quad \text{(A2)}$$

where $V_{m,EtOH}$ and V_{m,H_2O} are the partial molar volumes of ethanol and water, respectively, and n_{EtOH} and n_{H_2O} are the number of moles of ethanol and water, respectively. This can also be written in terms of the total volume of the droplet, V_{total}.

$$\%V_{EtOH} = \frac{V_{m,EtOH}n_{EtOH}}{V_{total}}100 \quad \text{(A3)}$$

Thus, the change in ethanol concentration by % v/v can be expressed as

$$\Delta\%V_{EtOH} = 100\left(\frac{V_{m,EtOH}n_{EtOH}}{V_{total}} - \frac{V^0_{m,EtOH}n^0_{EtOH}}{V^0_{total}}\right) \quad \text{(A4)}$$

Assuming that the compositional change is small, $V_{m,EtOH} \sim V^0_{m,EtOH}$

$$\Delta\%V_{EtOH} = 100\frac{V_{m,EtOH}}{V_{total}}\left(n_{EtOH} - \frac{V_{total}}{V^0_{total}}n^0_{EtOH}\right) \quad \text{(A5)}$$

To perform the gas-diffusional analysis presented here, we also make the more significant assumption that the change in droplet radius is small, $V_{total} \sim V^0_{total}$

$$\Delta\%V_{EtOH} \approx 100\frac{V_{m,EtOH}}{V_{total}}(n_{EtOH} - n^0_{EtOH}) \quad \text{(A6)}$$

The only time dependent variable is the number of moles of ethanol in the droplet, n_{EtOH}.

References and Notes

(1) Davis, E. J.; Schweiger, G. *The Airborne Microparticle*, Springer-Verlag: **2002**.
(2) Mønster, J.; Rosenørn, T.; Svenningsson, B.; Bilde, M. *J. Aerosol Sci.* **2004**, *35*, 1453.
(3) Vesala, T.; Kulmala, M.; Rudolf, R.; Vrtala, A.; Wagner, P. E. *J. Aerosol Sci.* **1997**, *28*, 565.
(4) Mattila, T.; Kulmala, M.; Vesala, T. *J. Aerosol Sci.* **1997**, *28*, 553.
(5) Devarakonda, R.; Ray, A. K. *J. Colloid Interface Sci.* **2000**, *221*, 104.
(6) Widmann, J. F.; Davis, E. J. *Aerosol Sci. Technol.* **1997**, *27*, 243.
(7) Ravindran, P.; Davis, E. J. *J. Colloid Interface Sci.* **1982**, *85*, 278.
(8) Shulman, M. L.; Charlson, R. J.; Davis, E. J. *J. Aerosol Sci.* **1997**, *28*, 737.
(9) Lightstone, J. M.; Onasch, T. B.; Imre, D. *J. Phys. Chem. A* **2000**, *104*, 9337.
(10) Tang, I. N.; Munkelwitz, H. R. *Aerosol sci. Technol.* **1991**, *15*, 201.
(11) Tang, I. N.; Munkelwitz, H. R. *J Geophys. Res. Atmos.* **1994**, *99*, 18801.
(12) Colberg, C. A.; Krieger, U. K.; Peter, T. *J. Phys. Chem. A* **2004**, *108*, 2700.
(13) Vehring, R.; Moritz, H.; Niekamp, D.; Schweiger, G.; Heinrich, P. *App. Spec.* **1995**, *49*, 1215.
(14) Buehler, M. F.; Allen, T. M.; Davis, E. J. *J. Colloid Interface Sci.* **1991**, *146*, 79.
(15) Tzeng, H. M.; Wall, K. F.; Long, M. B.; Chang, R. K. *Optics Lett.* **1984**, *9*, 273.
(16) Pastel, R.; Struthers, A. *Appl. Opt.* **2001**, *40*, 2510.
(17) Hopkins, R. J.; Symes, R.; Sayer, R. M.; Reid, J. P. *Chem. Phys. Lett.* **2003**, *380*, 665.
(18) Roman, V. E.; Popp, J.; Fields, M. H.; Kiefer, W. *J. Opt. Soc. Am. B* **1999**, *16*, 370.
(19) Kiefer. W.; Popp. J.; Lankers, M.; Trunk, M.; Hartmann, I.; Urlaub, E.; Musick, J. *J. Mol. Struct.* **1997**, *408/409*, 113.
(20) Qu, X.; Davis, E. J. *Aerosol. Sci.* **2001**, *32*, 861.
(21) Lin, H. B.; Eversole, J. D.; Campillo, A. J. *Opt. Commun.* **1990**, *77*, 407.
(22) Eversole, J. D.; Lin, H. B.; Huston, A. L.; Campillo, A. J.; Leung, P. T.; Liu, S. Y.; Young, K. *J. Opt. Soc. Am. B* **1993**, *10*, 1955.
(23) Biswas, A.; Latifi, H.; Armstrong, R. l. Pinnick, R. G. *Phys. Rev. A* **1989**, *40*, 7413.
(24) Sayer, R. M.; Gatherer, R. D. B.; Gilham, R. J. J.; Reid, J. P. *Phys. Chem. Chem. Phys.* **2003**, *5*, 3732.
(25) Campillo, A. J.; Eversole, J. D.; Lin, H. B. *J. Chem. Phys.* **1998**, *109*, 9199.
(26) Symes, R.; Sayer, R. M.; Reid, J. P. *Phys. Chem. Chem. Phys.* **2004**, *6*, 474.
(27) Symes, R.; Gilham, R. J.; Sayer. R. M.; Reid, J. P. *Phys. Chem. Chem. Phys.* **2005**, *7*, 1414.
(28) Hill, S. C.; Benner, R. E. *Morphology-Dependent Resonances*, ed. Barber, P. W.; Chang, R. K.; **1998**.
(29) Eversole, J. D.; Lin, H. B.; Campillo, A. J. *J. Opt. Soc. Am. B*, **1995**, *12*, 287.
(30) Berglund, R. N.; Liu, B. Y. H. *Environ. Sci. Technol.* **1973**, *7*, 147.
(31) Favre, C.; Boutou, V.; Hill, S. C.; Zimmer, W.; Krenz, M.; Lambrecht, H.; Yu, J.; Chang, R. K.; Woeste, L.; Wolf, J. *Phys. Rev. Lett.* **2002**, *89*, 035002.
(32) Khaled, E. E. M.; Hill, S. C.; Barber, P. W. *App. Opt.* **1994**, *33*, 524.
(33) Sayer, R. M.; Gatherer, R. D. B.; Reid, J. P. *Phys. Chem. Chem. Phys.* **2003**, *5*, 3740.
(34) *Handbook of Chemistry and Physics*, *84th Ed*. **2003**−**2004**, CRC Press LLC.
(35) Lavieille, P.; Lemoine, F.; Lavergne, G.; Virepinte, J. F.; Lebouche, M. *Exp. Fluids*, **2000**, *29*, 429.
(36) Qu, X.; Davis, E. J.; Swanson, B. D. *J. Aerosol Sci.* **2001**, *32*, 1315.
(37) Devarakonda, V.; Ray, A. K. *J. Aerosol. Sci.* **2003**, *34*, 837.
(38) Newbold, F. R.; Amundson, N. R. *AIChE Journal*, **1973**, *19*, 22.
(39) Shi, Q.; Li, Q.; Davidovits, P.; Jayne, J. T.; Worsnop, D. R.; Mozurkewich, M.; Kolb, C. E. *J. Phys. Chem. B* **1999**, *103*, 2417.
(40) Pinnick, R. G.; Biswas, A.; Chylek, P.; Armstrong, R. L.; Latifi, H.; Creegan, E.; Srivastava, V.; Jarzembski, M.; Fernandez, G. *Opt. Lett.* **1988**, *13*, 494.
(41) Zielkiewicz, J.; Konitz, A. *Fluid Phase Equilibria* **1991**, *63*, 129.
(42) Dobson, H. J. E. *J. Chem. Soc. Trans.* **1925**, *127*, 28771.
(43) D'Arrigo, G. D.; Maisano, G.; Mallamace, F.; Migliardo, P.; Wanderlingh, F. *J. Chem. Phys.* **1981**, *75*, 4264.
(44) Walrafen, G. E.; Hokmabadi, M. S.; Yang, W. H. *J. Chem. Phys.* **1986**, *85*, 6964.
(45) Hare, D. E.; Sorensen, C. M. *J. Chem. Phys.* **1990**, *93*, 25.
(46) Hopkins, R. J.; Mitchem, L.; Ward, A. D.; Reid, J. P. *Phys. Chem. Chem. Phys.* **2004**, *6*, 4924.